Monthly Notices
of the
ROYAL ASTRONOMICAL SOCIETY

MNRAS **493,** 6095–6108 (2020) doi:10.1093/mnras/staa653

Non-local thermodynamic equilibrium line formation for Si I–II–III in A–B stars and the origin of Si II emission lines in ι Her

Lyudmila Mashonkina★

Institute of Astronomy of the Russian Academy of Sciences, Pyatnitskaya st 48, 119017 Moscow, Russia

Accepted 2020 March 2. Received 2020 March 1; in original form 2020 January 21

ABSTRACT

A comprehensive model atom was developed for Si I–II–III using the most up-to-date atomic data available so far. Based on non-local thermodynamic equilibrium (NLTE) line formation for Si I, Si II and Si III and high-resolution observed spectra, we determined the NLTE abundances for a sample of nine unevolved A9–B3 type stars with well-determined atmospheric parameters. For each star, NLTE reduces the line-to-line scatter for Si II substantially compared with the LTE case and leads to consistent mean abundances from lines of different ionization stages. In the hottest star of our sample, ι Her, Si II is subject to overionization that drives emission in the lines arising from the high-excitation doublet levels. Our NLTE calculations reproduced 10 emission lines of Si II observed in ι Her. The same overionization effect leads to greatly weakened Si II lines, which are observed in absorption in ι Her. Large positive NLTE abundance corrections (up to 0.98 dex for 5055 Å) were useful for achieving consistent mean abundances from lines of the two ionization stages, Si II and Si III. It was found that NLTE effects are overestimated for the Si II 6347, 6371 Å doublet in ι Her, while the new model atom works well for cooler stars. At this stage, we failed to understand this problem. We computed a grid of the NLTE abundance corrections for lines of Si I, Si II and Si III in model atmospheres with effective temperatures and surface gravities characteristic of unevolved A–B type stars.

Key words: line: formation – stars: abundances – stars: atmospheres.

1 INTRODUCTION

Silicon is one of the most abundant metals. Analyses of the silicon lines in A- to mid B-type stars are important for addressing several problems. Such stars are young and can serve as indicators for present-day cosmic abundances. Using a sample of unevolved early B-type stars in nearby OB associations and field and non-local thermodynamic equilibrium (NLTE) line formation for Si III, Przybilla, Nieva & Butler (2008) and Nieva & Przybilla (2012) have established the Cosmic Abundance Standard and proved that the mean stellar silicon abundance agrees within 0.01 dex with the solar one. Fossati et al. (2009) investigate whether the chemical composition of the solar photosphere can also be regarded as a reference for early A- and late B-type stars. For each of their three stars, local thermodynamic equilibrium (LTE) analysis led to quite discordant abundances from lines of different ionization stages of silicon. Fossati et al. (2009) claim there is a real need for calculations based on NLTE line formation for Si I–Si II–Si III in A- to mid B-type stars.

In this exact range of spectral types, spectroscopic peculiarities (chemical abundance peculiarities, stratification, Zeeman effect, etc.) are frequent for stars. In order to quantify correctly the impact of the various physical processes that occur inside the atmospheres of such stars on the emergent spectra, one needs to test how the applied methods of spectral analysis allow one to fit the observations. Bailey & Landstreet (2013) determined LTE abundances from lines of the first and second ions of silicon in magnetic Bp and HgMn stars and used normal B stars of similar temperatures as a comparison sample. Both magnetic and non-magnetic stars show a discordance between Si II and Si III based abundances; however, the effect is much smaller for normal B-type stars, with the abundance difference Si III – Si II = 0.3–0.8 dex for different stars. Departures from LTE are suggested as a source of these discrepancies.

In A- to mid B-type stars, silicon can be observed in lines of two ionization stages: Si I and Si II if the star's effective temperature ($T_{\rm eff}$) is below approximately 11 000 K, and Si II and Si III for hotter stars. This is suitable for constraining and checking atmospheric parameters. For different temperatures, either Si I or Si II is a minority species, for which statistical equilibrium (SE) can easily deviate from thermodynamic equilibrium, owing to deviations of the mean intensity of ionizing radiation from the Planck function. Therefore, a correct evaluation of atmospheric parameters from the Si I/Si II or Si II/Si III ionization equilibrium method can only be possible when neglecting the LTE assumption.

★ E-mail: lima@inasan.ru

Sadakane & Nishimura (2017) and Sadakane & Nishimura (2019) registered weak emission lines of Si II in the red-region spectra of slowly rotating early B-type stars, HD 160762 (ι Her, B3 IV) among them. LTE calculations with a classical hydrostatic model atmosphere can only yield an absorption-line profile and never the emission one. Mihalas, Hummer & Conti (1972) were the first who showed that the emission lines (N III 4634, 4640, 4641 Å) in spectra of main-sequence objects (O stars with $T_{\rm eff} \geq 37\,000$ K) can be reproduced using classical hydrostatic model atmospheres, when taking NLTE effects on line formation into account. In ι Her, emission lines are observed for several chemical species (Sadakane & Nishimura 2019). For C I and Ca II, their emission lines are well reproduced in the NLTE calculations of Alexeeva, Ryabchikova & Mashonkina (2016) and Sitnova, Mashonkina & Ryabchikova (2018), respectively.

NLTE effects for Si I (and Si II, in some cases) are studied broadly for late-type and low-metallicity stars, using the model atoms treated by Vernazza, Avrett & Loeser (1976), Finn & McAllister (1978), Shi et al. (2008), Bard & Carlsson (2008), Shchukina, Sukhorukov & Trujillo Bueno (2012), Bergemann et al. (2013) and Amarsi & Asplund (2017). At the hottest end of the spectral-type sequence, early B and O, NLTE calculations for Si II, Si III and Si IV are performed with the model atoms constructed by Kamp (1978), Lennon et al. (1986) and Becker & Butler (1990). As for A- to mid B-type stars, very few estimates of NLTE abundances are based on the theoretical results of Wedemeyer (2001), who studied the Si II 3862, 4128–4130 and 5041–5056 Å lines in the benchmark star Vega.

This study aims to fill a gap in theoretical research into line formation in stellar atmospheres and to develop a NLTE method for analysis of Si I, Si II and Si III lines in spectra of A- to mid B-type stars. For a sample of nine unevolved A9- to B3-type stars with well-determined atmospheric parameters, we investigated whether we can obtain, for each star, consistent abundances from different lines of silicon in different ionization stages. A challenge for this study was understanding the origin of the Si II emission lines in ι Her.

The article is organized as follows. The new model atom for Si I–II–III is presented in Section 2. Our stellar sample, observational material and adopted atmospheric parameters are described briefly in Section 3. NLTE effects on atomic level populations and lines of Si I, Si II and Si III are discussed in Section 4. Section 5 presents the abundance results for eight stars with $T_{\rm eff} \leq 12\,800$ K. Section 6 is devoted to our hottest star, ι Her, with its emission lines of Si II. Having convinced ourselves that the NLTE method works well for Si I–II–III through a range of A–B spectral types, in Section 7 we compute the NLTE abundance corrections for silicon lines in the grid of model atmospheres. Our conclusions are summarized in Section 8.

2 MODEL ATOM OF Si I–Si II–Si III

2.1 Energy levels

For Si I, we employ all 451 energy levels below the ionization threshold, $\chi_{\rm thr,\,1} = 65\,736.06$ cm^{-1} $= 8.187$ eV, provided by the National Institute of Standards and Technology (NIST)[1] database (Kramida et al. 2019) based on the data of Martin & Zalubas (1983) and also 268 high-excitation levels, which are predicted by R. Kurucz[2] in calculations of Si I atomic structure but which are missing in NIST. The model atom includes the multiplet fine structure for all terms up to Si I 3p5s ^{3}P$^\circ$, with an excitation energy of $E_{\rm exc} = 6.725$ eV. For $E_{\rm exc} > 7.96$ eV levels, a combining procedure was applied, if the levels have a common parity and the energy separation does not exceed 0.037 eV (300 cm^{-1}). Thus, 95 levels in our model atom of Si I were made using the NIST data and 23 levels using Kurucz's predictions.

For Si II and Si III, the same sources of data were used as for Si I. NIST provides 93 energy levels of Si II below the ionization threshold, $\chi_{\rm thr,\,2} = 131\,838.14$ cm^{-1} $= 16.346$ eV. Taking into account the multiplet fine structure for the Si II ground (3p ^{2}P$^\circ$) and first excited (3p^2 ^{4}P) terms and neglecting it for all other terms, we obtained 50 levels. We also implemented the 28 high-excitation levels predicted by R. Kurucz, which were combined into six levels. Our model atom of Si II is complete up to principal quantum number $n = 9$ and orbital quantum number $l = 7$ and includes terms with $l \leq 4$ for $n = 10$ and 11.

For Si III, NIST provides 177 energy levels of the 3snl ($n \leq 9$, $l \leq 8$) and 3pnl ($n \leq 4$, $l \leq 2$) electronic configurations. Neglecting the multiplet fine structure for all terms except the first excited one, 3p ^{3}P$^\circ$, we obtained 54 levels in the model atom of Si III.

For $T_{\rm eff} < 10\,000$ K, the NLTE calculations were performed with a reduced model atom, which includes levels of Si I, Si II and the ground state of Si III, because, in such atmospheres, a fraction of Si III is small and no Si III line can be detected in $T_{\rm eff} < 10\,000$ K stars. For higher temperatures, we used a model atom that includes four ionization stages, that is Si I, Si II, Si III and the ground state of Si IV.

2.2 Radiative bound–bound (b–b) transitions

We do not take into account radiative transitions with either wavelength $\lambda > 300\,000$ Å or oscillator strength $f_{lu} < 10^{-6}$. Finally, radiative rates were computed for 1814, 475 and 327 allowed transitions of Si I, Si II and Si III, respectively. Their f_{lu} values were taken from the calculations of R. Kurucz. In cases in which either the lower or/and upper level of the transition is combined, the average 'multiplet' oscillator strength was calculated as $f_{lu} = \Sigma g_i f_{ij} / g_l$, where summing is performed for all levels i and j, which constitute the levels l and u, respectively; g_i and g_l are the statistical weights of the levels i and l.

2.3 Radiative bound–free (b–f) transitions

For the 55 lowest levels of Si I with angular momentum $L \leq 3$, up to 3p7s ^{3}P$^\circ$ (the threshold wavelength is $\lambda_{\rm thr} = 24\,000$ Å), 41 levels of Si II ($L \leq 4$, up to 9p ^{2}P$^\circ$ with $\lambda_{\rm thr} = 14\,690$ Å) and 40 levels of Si III up to 7d ^{3}D ($\lambda_{\rm thr} = 4742$ Å), we rely on the photoionization cross-sections calculated within the Opacity Project (OP: Seaton 1987) and accessible in the TOPbase[3] database (Cunto et al. 1993). For the remaining levels in the model atom, the hydrogenic approximation was used, with effective principal quantum number $n_{\rm eff}$ instead of n.

We note that the photoionization cross-sections computed by Nahar (2000) and Nahar (1995) for Si I and Si II, respectively, as available in the NORAD[4] database, are very similar to the

[1] https://physics.nist.gov/PhysRefData/ASD

[2] http://kurucz.harvard.edu/atoms/

[3] http://cdsweb.u-strasbg.fr/cgi-bin/topbase/

[4] https://norad.astronomy.osu.edu/

Table 1. Atmospheric parameters of the sample stars and mean NLTE (N) and LTE (L) abundances from lines of different ionization stages of silicon.

HD	$T_{\rm eff}$ [K]	log g	[Fe/H]	$\xi_{\rm t}$	Ref		Si I		Si II		Si III		[Si/H]
							N_l	log ε	N_l	log ε	N_l	log ε	
32115	7250	4.20	0.00	2.3	F11	N	16	7.58(0.17)	4	7.65(0.08)			0.10
						L		7.61(0.17)		7.82(0.24)			
73666	9380	3.78	0.10	1.8	F07	N	1	7.54	13	7.68(0.17)			0.10
(40 Cnc)						L		7.16		7.84(0.26)			
172167	9550	3.95	−0.50	1.8	C93	N			8	6.92(0.15)			−0.59
(Vega)						L				7.08(0.17)			
72660	9700	4.10	0.40	1.8	S16	N	6	7.85(0.04)	14	7.82(0.11)			0.33
						L		7.59(0.09)		7.94(0.23)			
145788	9750	3.70	0.46	1.3	F09	N			7	7.63(0.12)			0.12
						L				7.90(0.19)			
48915	9850	4.30	0.40	1.8	H93	N	1	7.59	11	7.72(0.11)			0.21[1]
(Sirius)						L		7.26		7.84(0.18)			
209459	10400	3.55	0.00	0.5	F09	N	1	7.49	17	7.50(0.13)			−0.01
(21 Peg)						L		7.08		7.62(0.29)			
17081	12800	3.75	0.00	1.0	F09	N			19	7.75(0.14)	2	7.72(0.04)	0.23
(π Cet)						L				7.59(0.25)		7.82(0.00)	
160762	17500	3.80	0.02	1.0	N12	N			13	7.74(0.25)[2]	4	7.54(0.07)	0.03[3]
(ι Her)						L				7.07(0.41)[2]		7.79(0.05)	

Notes. The numbers in parentheses are the dispersions in the single line measurements around the mean. $\xi_{\rm t}$ is in km s^{-1}.
[1] based on Si II lines; [2] Si II 6347, 6371 Å and emission lines are not accounted for in the mean; [3] based on Si III lines.
Ref: C93 = Castelli & Kurucz (1993); F07, F09, F11 = Fossati et al. (2007, 2009, 2011);
H93 = Hill & Landstreet (1993); N12 = Nieva & Przybilla (2012); S16 = Sitnova, Mashonkina & Ryabchikova (2016).

TOPbase ones for photon energies close to the ionization threshold within approximately 0.5 Ryd and they are systematically smaller at higher photon energies, by 0.1–0.5 dex for different levels. Singh et al. (2011) calculated for the first time the photoionization cross-sections for the fine-splitting levels of the Si II $3s^23p\,^2P^\circ$, $3s3p^2\,^4P$ and $3s3p^2\,^2D$ terms. Since these data are not available in tabular form, they cannot be checked in our NLTE calculations. However, we note that, in the stellar parameter range with which this study is concerned, photoionization of the $3s^23p\,^2P^\circ$ and $3s3p^2\,^4P$ terms affects the SE of Si II only weakly. For Si II $3s3p^2\,^2D$, the photoionization cross-sections in figs 6 and 7 of Singh et al. (2011) are smaller than the TOPbase ones for photon energies below 1.2 Ryd and resemble the predictions of Nahar (1995).

2.4 Collisional transitions

For Si I, the electron-impact excitations are not yet known with sufficient accuracy and our calculations of collisional rates rely on theoretical approximations. We used the formula of van Regemorter (1962) for allowed transitions and assumed that the effective collision strength $\Upsilon = 1$ for forbidden transitions. For 414 transitions between terms up to $3s3p3d\,^2P^\circ$ in Si II (28 per cent of the total number of collisional transitions in Si II) and 210 transitions between terms up to $3p3d\,^1F^\circ$ in Si III (15 per cent of the total number of collisional transitions in Si III), we employed data from the **R**-matrix calculations of Aggarwal & Keenan (2014) and Fernández-Menchero, Del Zanna & Badnell (2014), respectively. The same formulae as for Si I were applied for the remaining transitions in Si II and Si III. Ionization by electronic collisions was calculated everywhere from the Seaton (1962) formula with a hydrogenic photoionization cross-section at the threshold.

The effects of uncertainties in atomic data on the NLTE results are discussed in Section 6, using the silicon emission and absorption lines in ι Her.

3 STELLAR SAMPLE, OBSERVATIONS AND ATMOSPHERIC PARAMETERS

As a test and first application of the model atom, silicon lines in nine objects were analysed. This research continues a series of NLTE studies of chemical species in A–B type stars, namely O I (Sitnova, Mashonkina & Ryabchikova 2013), C I–II (Alexeeva et al. 2016), Ti I–II (Sitnova et al. 2016), Mg I–II (Alexeeva et al. 2018) and Ca I–II (Sitnova et al. 2018). Therefore, we take the same stellar sample, with their atmospheric parameters and the same spectral observations. The selected stars, their effective temperatures, surface gravities (log g), metallicities ([Fe/H]) and microturbulent velocities ($\xi_{\rm t}$) and the sources of these data are listed in Table 1.

Alexeeva et al. (2016) described the programme stars in detail; we summarize briefly here. Only sharp-lined stars, with rotational velocities of $V \sin i \lesssim 20$ km s^{-1}, were included in our sample, in order to perform spectral analysis at the highest precision.

The stars 21 Peg and ι Her are chemically normal single stars.

Each of HD 32115, HD 73666 and π Cet is a primary component of a single-line spectroscopic binary (SB1), with negligible flux coming from the secondary star. Therefore, it is safe to analyse these stars ignoring the presence of their secondaries. For none of them was a chemical peculiarity reported. HD 73666 is a blue straggler and a member of the Praesepe cluster.

HD 145788 reveals an overabundance of almost all metals, according to Fossati et al. (2009). They conclude that its element abundance pattern 'could be explained if HD 145788 was formed in a region of the sky with a metallicity higher than the solar region'.

Sirius is an astrometric visual binary system composed of a main-sequence A1V star and a DA white dwarf. The primary component is classified as a metallic-line (Am) star.

HD 72660 was classified by Golriz & Landstreet (2016) as a transition object between an HgMn star and an Am star.

Vega is a rapidly rotating star seen pole-on and is also classified as a mild λ Bootis type star. Similarly to our previous studies, we

ignore non-spherical effects and analyse Vega's flux spectrum using the average temperature and gravity.

We refer to the original articles and also Alexeeva et al. (2016, 2018) and Sitnova et al. (2016) for a description of the methods of atmospheric parameter determination.

For seven of the nine stars, observational material for the visual spectral range was obtained with a spectral resolving power of $R = \lambda/\Delta\lambda > 60\,000$ and a signal-to-noise ratio of S/N > 200, using the ESPaDOnS instrument of the Canada–France–Hawaii Telescope (CHFT). Vega was observed by A. Korn using the spectrograph FOCES(fibre optics Cassegrain echelle spectrograph) ($R \simeq 40\,000$, S/N > 750) at the 2.2-m telescope of the Calar Alto Observatory. HD 145788 was observed with the échelle spectrograph HARPS(High Accuracy Radial velocity Planet Searcher) instrument ($R \simeq 115\,000$, S/N $\simeq$ 200) attached at the 3.6-m ESO La Silla telescope. For HD 72660, we also use the UV spectrum kindly provided by J. Landstreet. The observations and spectrum reduction are described by Golriz & Landstreet (2016).

4 NLTE CALCULATIONS

4.1 Codes, model atmospheres, list of investigated lines

The coupled radiative transfer and SE equations were solved with a modified version of the DETAIL code (Butler & Giddings 1985; Przybilla, Nieva & Butler 2011). As verified by Przybilla et al. (2011), a hybrid method combining LTE atmospheres and NLTE line formation is able to reproduce observations for effective temperatures between 15 000 and 35 000 K. This is all the more true for cooler atmospheres. For consistency with our earlier studies, for each star we used exactly the same model atmosphere. Classical plane-parallel and LTE model atmospheres were calculated with the code LLMODELS (Shulyak et al. 2004). For Sirius, its model atmosphere was taken from the website of R. Kurucz.[5]

The line lists of Fossati et al. (2009, 2011) and Sadakane & Nishimura (2019) were used to select the silicon lines for NLTE analysis. The sample of lines observed in stellar spectra changes substantially when moving from our coolest to our hottest star. Therefore, the lines used, together with their atomic parameters, are listed in five separate tables: Si I and Si II lines in HD 32115 (Table 2), Si I UV lines (Table 3), Si I and Si II lines in the visible spectra of eight stars with $T_{\rm eff} > 9000$ K (Table 4), Si III lines (Table 5) and Si II emission lines in ι Her (Table 6). For lines of Si III, quadratic Stark effect broadening was taken into account using the approximate formula of Cowley (1971).

In this research, analysis of observed spectra is based on line-profile fitting. The synthetic spectra were computed with the SYNTHV_NLTE code (Tsymbal, Ryabchikova & Sitnova 2019), which implements the pre-computed departure coefficients from the DETAIL code. We note that SYNTHV_NLTE treats the contribution of the overlapping hydrogen Balmer lines to the background opacity using occupation probability theory, as developed by Hummer & Mihalas (1988), Hubeny, Hummer & Lanz (1994) and Nayfonov et al. (1999). This is important for calculations of Si I 3905 Å and Si II 3853, 3856, 3862 Å. The best fit to the observed spectrum was obtained automatically using the IDL BINMAG code by O. Kochukhov.[6] The line list and atomic data for the synthetic spectra calculations were taken from the VALD(Vienna Atomic Line Database) database (Ryabchikova et al. 2015).

[5] http://kurucz.harvard.edu/stars/sirius/ap04t9850g43k0he05y.dat
[6] http://www.astro.uu.se/~oleg/binmag.html

Table 2. NLTE (N) and LTE (L) abundances, $\log\varepsilon$, from lines of Si I and Si II in the Sun and HD 32115.

Transition	λ [Å]	log *gf*		Sun	HD 32115
Si I					
$4s\,^3P^\circ$–$5p\,^3P$	5690.42	−1.87[1]	N	7.64	7.55
$E_{\rm exc}$ = 4.93 eV			L	7.66	7.57
$4s\,^1P^\circ$–$5p\,^1S$	5772.15	−1.75[1]	N	7.65	7.60
$E_{\rm exc}$ = 5.08 eV			L	7.67	7.61
$4s\,^1P^\circ$–$5p\,^1D$	5948.54	−1.23[1]	N	7.64	7.64
$E_{\rm exc}$ = 5.08 eV			L	7.69	7.67
$3p^3\,^3D^\circ$–$5f\,^3D$	6142.48	−1.30[2]	N	7.37	7.40
$E_{\rm exc}$ = 5.62 eV			L	7.39	7.41
$3p^3\,^3D^\circ$–$5f\,^3G$	6155.13	−0.76[2]	N	7.46	7.42
$E_{\rm exc}$ = 5.62 eV			L	7.50	7.44
$3p^3\,^3D^\circ$–$5f\,^3F$	6237.32	−0.98[2]	N	7.40	7.39
$E_{\rm exc}$ = 5.61 eV			L	7.42	7.41
$3d\,^1D^\circ$–6f2[7/2]	6414.98	−1.04[2]	N	7.51	7.51
$E_{\rm exc}$ = 5.87 eV			L	7.53	7.53
$4p\,^1P$–$6d\,^1D^\circ$	6721.85	−0.94[3]	N	7.36	7.31
$E_{\rm exc}$ = 5.86 eV			L	7.38	7.33
$4p\,^3D$–$6d\,^3P^\circ$	6741.63	−1.75[2]	N	7.68	7.80
$E_{\rm exc}$ = 5.98 eV			L	7.70	7.83
$4p\,^1P$–7s(3/2,1/2)°	6848.58	−1.53[2]	N	7.42	7.32
$E_{\rm exc}$ = 5.86 eV			L	7.43	7.34
$3d\,^1D^\circ$–5f2[7/2]	7034.90	−0.88[2]	N	7.64	7.57
$E_{\rm exc}$ = 5.87 eV			L	7.68	7.61
$4p\,^3D$–7s(3/2,1/2)°	7373.00	−1.18[2]	N	7.43	7.37
$E_{\rm exc}$ = 5.98 eV			L	7.43	7.39
$3p^3\,^3D^\circ$–$4f\,^3F$	7405.77	−0.82[2]	N	7.61	7.65
$E_{\rm exc}$ = 5.61 eV			L	7.67	7.70
$4p\,^1P$–$5d\,^1D^\circ$	7680.27	−0.69[1]	N	7.65	7.57
$E_{\rm exc}$ = 5.86 eV			L	7.71	7.61
$3d\,^3F^\circ$–6f2[5/2]	7849.97	−0.71[2]	N	7.50	7.50
$E_{\rm exc}$ = 6.19 eV			L	7.53	7.53
$4p\,^3D$–$5d\,^3F^\circ$	7944.00	−0.31[1]	N	7.62	7.56
$E_{\rm exc}$ = 5.98 eV			L	7.72	7.64
Si II					
$4p\,^2P^\circ$–$4d\,^2D$	5055.98	0.52[4]	N		7.68
$E_{\rm exc}$ = 10.07 eV			L		7.68
$4p\,^2P^\circ$–$5s\,^2S$	5978.93	0.08[5]	N		7.58
$E_{\rm exc}$ = 10.07 eV			L		7.58
$4s\,^2S$–$4p\,^2P^\circ$	6347.11	0.15[4]	N	7.62	7.75
$E_{\rm exc}$ = 8.12 eV			L	7.72	8.04
	6371.37	−0.08[4]	N	7.50	7.64
			L	7.58	7.86

Notes: [1] Garz (1973), [2] VALD, [3] Wiese, Smith & Miles (1969), [4] Matheron et al. (2001), [5] Blanco, Botho & Campos (1995).

Table 3. NLTE and LTE abundances, $\log\varepsilon$, from the UV lines of Si I and Si II in HD 72660.

Transition	λ [Å]	$E_{\rm exc}$ [eV]	log *gf*	NLTE	LTE
Si I					
$3p\,^3P$–$5d\,^1D^\circ$	1664.51	0.03	−1.80	7.86	7.66
$3p\,^3P$–$5d\,^3P^\circ$	1666.38	0.00	−1.66	7.84	7.54
$3p\,^3P$–$6s\,^1P^\circ$	1682.67	0.01	−1.85	7.91	7.64
$3p\,^3P$–$6s\,^3P^\circ$	1689.29	0.01	−1.83	7.88	7.66
$3p\,^3P$–$4d\,^3D^\circ$	1699.72	0.03	−2.63	7.82	7.58
Si II					
$3p^2\,^2D$–$5f\,^2F^\circ$	1710.84	6.86	−0.57	7.97	7.97

Notes: *gf* values are from Smith et al. (1987) for Si I and from VALD for Si II.

Table 4. NLTE (N) and LTE (L) abundances, $\log \varepsilon$, from lines of Si I and Si II in the sample stars.

Transition (E_{exc})	λ [Å]	log *gf*	Ref	log Γ_4/N_e		HD 73666	Vega	HD 72660	HD 145788	Sirius	21 Peg	π Cet	ι Her
Si I													
$3p\,^1S_0$–$4s\,^1P^\circ_1$	3905.52	−1.04	O91	−5.60[1]	N	7.54		7.79		7.59	7.49		
(1.91 eV)					L	7.16		7.42		7.26	7.08		
Si II													
$3p^2\,^2D$–$4p\,^2P^\circ$	3853.67	−1.34	M01	−5.20[1]	N	7.63				7.67	7.50	7.81	7.85
(6.86 eV)					L	7.64				7.66	7.50	7.49	7.25
	3856.02	−0.41	M01	−5.24[1]	N	7.89				7.84	7.60	7.84	8.03
					L	7.89				7.84	7.62	7.68	7.48
	3862.59	−0.76	M01	−5.30[1]	N	7.94		7.94		7.85	7.69	7.93	7.98
					L	7.95		7.96		7.85	7.69	7.73	7.37
$3d\,^2D$–$5p\,^2P^\circ$	4075.45	−1.40	M01	−4.89[2]	N	7.52		7.78			7.53	7.65	7.67
(9.84 eV)					L	7.52		7.77			7.54	7.48	7.33
	4076.78	−1.68	M01	−4.89[2]	N							7.71	
					L							7.57	
$3d\,^2D$–$4f\,^2F^\circ$	4128.05	0.36	M01	−4.96[1]	N	7.53	6.87			7.64		7.48	7.25
(9.84 eV)					L	7.59	6.95			7.71		7.47	6.84
	4130.89	0.55	M01	−4.91[1]	N	7.54	6.85	7.72		7.59	7.32	7.48	7.15
	4130.87	−0.78			L	7.61	6.93	7.78		7.68	7.48	7.43	6.76
$4d\,^2D$–$7f\,^2F^\circ$	4621.42	−0.61	M95	−3.86[3]	N			7.78			7.50	7.75	b[4]
(12.52 eV)					L			7.76			7.44	7.56	
	4621.72	−0.45	M95		N			7.78			7.51	7.75	7.60
	4621.70	−1.75	M95		L			7.76			7.46	7.56	6.95
$4p\,^2P^\circ$–$4d\,^2D$	5041.02	0.03	M01	−4.80[1]	N	7.85		8.00	7.81	7.88	7.68	7.97	7.94
(10.07 eV)					L	7.93		8.06	7.94	7.93	7.80	7.78	6.97
	5055.98	0.52	M01	−4.76[1]	N	7.65	6.92	7.77	7.60	7.75	7.45	7.79	7.66
					L	7.76	6.96	7.86	7.76	7.81	7.60	7.58	6.68
	5056.32	−0.49	M01	−4.76[1]	N	7.73		7.85	7.69		7.56		7.78
					L	7.76		7.88	7.74		7.60		6.91
$4d\,^2D$–$6f\,^2F^\circ$	5466.89	−0.08	M95	−4.20[3]	N								7.75
(12.52 eV)	5466.85	−1.38	M95		L								6.57
$5p\,^2P^\circ$–$7d\,^2D$	5469.45	−0.76	M95	−4.06[3]	N							7.88	
(12.88 eV)	5469.47	−1.72	M95		L							7.40	
$4p\,^2P^\circ$–$5s\,^2S$	5957.56	−0.22	B95	−4.83[1]	N	7.62	6.96	7.71	7.63	7.68	7.36	7.74	7.60
(10.07 eV)					L	7.70	7.01	7.77	7.76	7.74	7.46	7.63	6.77
	5978.93	0.08	B95	−4.85[1]	N	7.55	6.87	7.69	7.57	7.64	7.32	7.63	7.57
					L	7.65	6.93	7.78	7.74	7.72	7.48	7.57	6.74
$4f\,^2F^\circ$–$6g\,^2G$	6239.61	0.18	M95	−3.54[3]	N			7.85			7.57	7.73	7.92
(12.84 eV)	6239.61	−1.12	M95		L			7.82			7.41	7.33	e[5]
	6239.66	0.02	M95										
$4s\,^2S$–$4p\,^2P^\circ$	6347.11	0.15	M01	−5.08[1]	N	7.60	6.80	7.79	7.55	7.69	7.28	7.77	8.38
(8.12 eV)					L	8.20	7.32	8.31	8.14	8.14	8.06	7.99	7.78
	6371.37	−0.08	M01	−5.08[1]	N	7.52	6.77	7.75	7.47	7.59	7.24	7.66	8.27
					L	8.09	7.12	8.15	8.04	7.95	7.89	7.84	7.60
$5p\,^2P^\circ$–$6d\,^2D$	6818.41	−0.52	M95	−4.24[3]	N								7.94
(12.88 eV)	6829.80	−0.26	M95		N							7.78	7.87
	6829.83	−1.22	M95		L							7.34	e
$4d\,^2D$–$5f\,^2F^\circ$	7848.82	0.32	M95	−4.68[3]	N						7.52	7.55	8.36
(12.52 eV)					L						7.32	7.14	e
	7849.72	0.47	M95		N						7.48	7.64	8.29
	7849.62	−0.83	M95		L						7.28	7.23	e

Notes: Γ_4/N_e in rad·s^{-1}·cm^{-3}, [1]Bukvić, Djeniže & Srećković (2009); [2]Wilke (2003, PhD thesis) as given by Fossati et al. (2009); [3]VALD; [4]blend; [5]emission line.
Ref. B95 = Blanco et al. (1995), M01 = Matheron et al. (2001), M95 = Mendoza et al. (1995), O91 = O'Brian & Lawler (1991).

4.2 Statistical equilibrium of silicon depending on effective temperature

For the energy levels, which are important for understanding the formation of the silicon lines observed in our sample stars, Fig. 1 displays the departure coefficients, $b = n_{NLTE}/n_{LTE}$, in four model atmospheres with different T_{eff}. Here, n_{NLTE} and n_{LTE} are the statistical equilibrium and thermal (Saha–Boltzmann) number densities, respectively. In our coolest atmosphere ($T_{eff}/\log g$ = 7250 K/4.20), silicon is strongly ionized, with N(Si II)/N(Si I) >30. For Si I, departures from LTE take place above the continuum optical depth $\log \tau_{5000} \simeq -1$. Superthermal radiation of a non-local origin below the thresholds of the Si I levels, such as $3p^2\,^1D$ (λ_{thr} = 1682 Å), $3p4s\,^1P^\circ$ (λ_{thr} = 4039 Å) and $3p3d\,^1D^\circ$ (λ_{thr} = 5435 Å), tends to overionize Si I. However, bound–bound transitions from many levels close to the ionization limit down to the lower levels can

Table 5. NLTE and LTE abundances, log ε, from lines of Si III in π Cet and ι Her.

λ [Å]	E_{exc} [eV]	log gf	π Cet		ι Her	
			NLTE	LTE	NLTE	LTE
4552.62	19.02	0.29			7.47	7.82
4567.84	19.02	0.07	7.69	7.82	7.52	7.80
4574.76	19.02	−0.41	7.74	7.82	7.52	7.70
5739.73	19.72	−0.10			7.63	7.81

Note: *gf* values are from NIST.

siphon an efficient flow of electrons downward. It increases the populations of the ground state, $3p^2\,^3P$, and low-lying levels, such as $3p^2\,^1S$ and $3p4s\,^1P^\circ$, above their thermodynamic equilibrium (TE) values, but depopulates high-excitation ($E_{exc} \gtrsim 6$ eV) levels, such as $3p5d\,^3P^\circ$ (in the top panel of Fig. 1, it is quoted as $5d\,^3P^\circ$ for brevity). The levels above $3d\,^2D$ in Si II are underpopulated ($b < 1$) by photon losses in transitions to lower levels as soon as the line centre optical depth drops below 1. Two transitions from the ground state to $4s\,^2S$ ($\lambda = 1526$, 1533 Å) are nearly in detailed balance throughout the atmosphere. This explains why the population of $4s\,^2S$ is close to the TE value.

In the hotter model atmosphere (9700/4.10), no processes in Si I can compete with overionization of the low-lying levels, resulting in strong depopulation of all the Si I levels. Si II remains a majority species and its ground state keeps the TE population throughout the atmosphere. Below log $\tau_{5000} \simeq -1$, the most important transitions of Si II are in detailed balance and the departure coefficients of the excited levels are close to 1. In the higher atmospheric layers, strong pumping transitions $3p\,^2P^\circ$–$4s\,^2S$ ($\lambda = 1526$, 1533 Å) and $3p\,^2P^\circ$–$3d\,^2D$ ($\lambda = 1260$, 1264 Å) produce enhanced excitation of the upper levels, while photon losses in the transitions to low-lying levels depopulate $4p\,^2P^\circ$ and the levels above.

Si I is strongly overionized in the two hottest models, 12 800/3.75 and 17 500/3.80, which represent the atmospheres of π Cet and ι Her. Since no lines of Si I can be measured in these stars, levels of Si I are not shown in Fig. 1. In the 12 800/3.75 model, Si II and Si III have comparable number densities in the line-formation layers, above log $\tau_{5000} = 0$. Superthermal radiation below the thresholds of the Si II levels, such as $4s\,^2S$ ($\lambda_{thr} = 1507$ Å), $3d\,^2D$ ($\lambda_{thr} = 1905$ Å) and $3p^2\,^2D$ ($\lambda_{thr} = 1306$ Å), leads to an overionization of Si II but enhanced populations of the Si III levels.

In the 17 500/3.80 model, Si II is subject to strong overionization, while Si III is a majority species. Its ground state keeps close to the TE population throughout the atmosphere. Pumping UV transitions from the low-excitation levels produce enhanced excitation of the lower level of the Si III $4s\,^3S$–$4p\,^3P^\circ$ transition (triplet lines at 4552, 4567 and 4574 Å) above log $\tau_{5000} \simeq 0$, while the upper level is depopulated via spontaneous transitions.

4.3 Non-LTE effects on spectral lines

Tables 2, 3, 4 and 5 and Figs 2 and 3 present the NLTE and LTE abundances from individual lines in the sample stars.

4.3.1 Lines of Si I

The 16 lines of Si I were measured in our coolest star, HD 32115 (Table 2, Fig. 2). They all arise from the $E_{exc} < 6.2$ eV levels, for which $b > 1$ in the line-formation layers, while populations of their upper levels are lower than the LTE ones. Therefore,

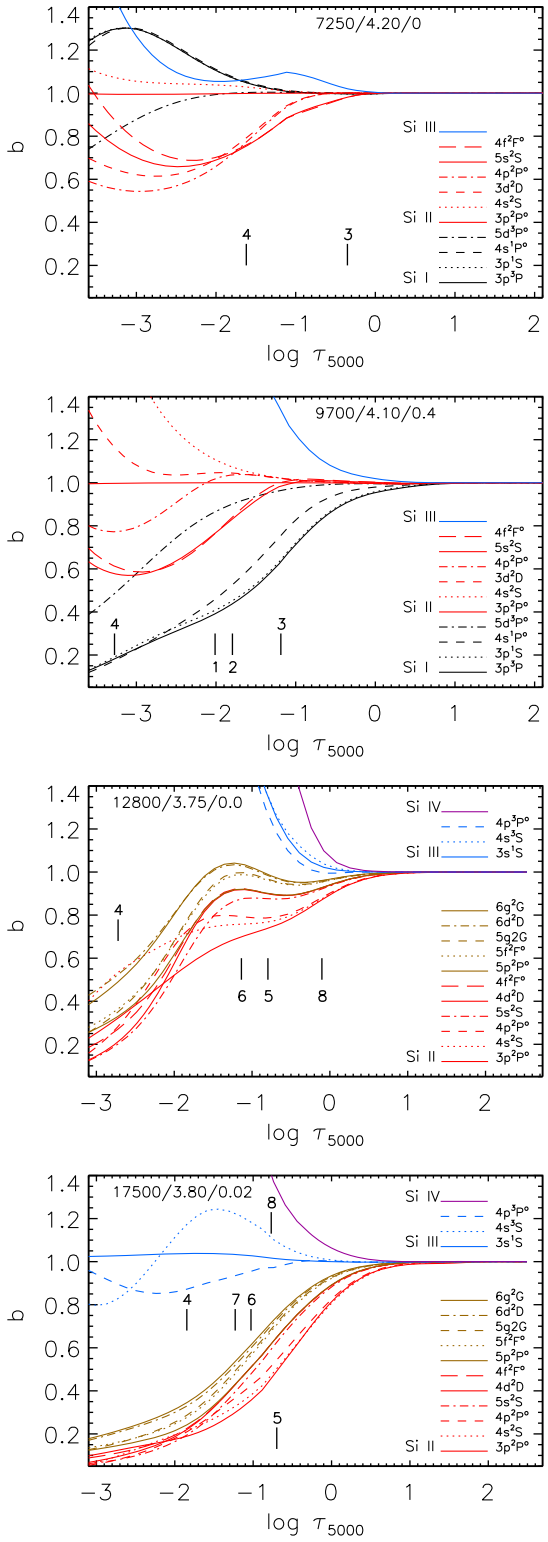

Figure 1. Departure coefficients, b, for the levels of Si I (black curves, two top panels), Si II (red and brown curves), Si III (blue curves) and Si IV (lilac curves) as a function of log τ_{5000} in the model atmospheres 7250/4.20/0, 9700/4.10/0.4, 12800/3.75/0.0 and 17500/3.80/0.02. The selected levels are quoted in the right part of each panel. Tick marks indicate the locations of line centre optical depth unity for the following lines: Si I 1666 (1) and 3905 Å (2), Si II 5957 (3), 6347 (4), 6239 (5), 7848 (6) and 9412 Å (7), and Si III 4567 Å (8).

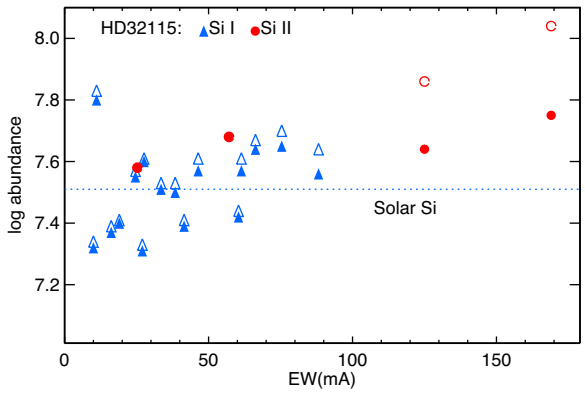

Figure 2. NLTE (filled symbols) and LTE (open symbols) abundances from lines of Si I (triangles) and Si II (circles) in HD 32115.

the lines are strengthened in NLTE and the NLTE abundance corrections, $\Delta_{\rm NLTE} = \log \varepsilon_{\rm NLTE} - \log \varepsilon_{\rm LTE}$, are negative. However, the NLTE effects are small, so that $\Delta_{\rm NLTE}$ ranges between −0.02 and −0.06 dex for different lines.

In the hotter, 9380 $\leq T_{\rm eff} \leq$ 10400 K, stars, only Si I 3905 Å was measured in the visible spectral range. We note that the observed spectra of Vega and HD 145788 do not cover this line. Overionization of Si I leads to a weakened line (Fig. 4) and large positive NLTE abundance correction, which ranges between 0.33 and 0.41 dex for different stars. Si I 3905.523 Å is blending with the Cr II 3905.644 Å line. However, as shown in Fig. 4, a variation of 0.1 dex in the Cr abundance does not influence the derived silicon abundance.

We are lucky to measure five lines of Si I in the UV spectrum of HD 72660 (Table 3). Their NLTE abundances agree well with that from Si I 3905 Å, so that the dispersion in the single line measurements around the mean, $\sigma = \sqrt{\Sigma(\overline{x} - x_i)^2/(N_l - 1)}$, amounts to 0.04 dex (Table 1). Here, N_l is the number of measured lines. This provides evidence for a reliable abundance from Si I 3905 Å, despite blending with Cr II 3905 Å.

4.3.2 Absorption lines of Si II

The Si II multiplets in Table 4 can be separated into three groups with respect to departures from LTE.

1. Si II 3853–3862 Å, 4075–4076 Å, 4128–4130 Å, 5041–5056 Å and 5957–5978 Å. In model atmospheres with $T_{\rm eff} \leq$ 10 400 K, where Si II is a majority species, the lower and upper levels of the corresponding transitions are tightly coupled to the ground state in the line-formation region, below $\log \tau_{5000} \simeq -2$ (see Fig. 1). As a result, NLTE effects are small, while $\Delta_{\rm NLTE}$ is slightly negative and does not exceed 0.02 dex for the two bluest multiplets and 0.16 dex for the remaining ones. In the atmospheres of π Cet and ι Her, all these lines are weakened due to overionization of Si II and the NLTE abundance corrections are positive. For example, they amount to 0.34–0.98 dex for different lines in ι Her.

2. Si II 6347, 6371 Å. In model atmospheres with $T_{\rm eff} \leq$ 12 800 K, NLTE leads to strengthened lines (Fig. 5 for 6371 Å) owing to dropping the line source function (S_ν) below the Planck function (B_ν) in the line-formation layers (see Fig. 1). NLTE effects grow toward higher effective temperature, so that, for Si II 6371 Å, the magnitude of $\Delta_{\rm NLTE}$ increases from −0.22 dex in HD 32115 to −0.65 dex in 21 Peg. In the atmosphere of π Cet, overionization of Si II competes with dropping S_ν/B_ν; however, the latter effect prevails, resulting in $\Delta_{\rm NLTE} = -0.18$ dex. Overionization of Si II is the dominant NLTE mechanism in the atmosphere of the hottest star, so that the Si II 6347, 6371 Å lines are greatly weakened and $\Delta_{\rm NLTE} = 0.60$ and 0.67 dex, respectively.

3. High-excitation ($E_{\rm exc} > 12$ eV) lines are observed in the three hottest stars. The exception is Si II 4621.4, 4621.7 Å and 6239 Å in HD 72660, which were measured thanks to narrower lines compared with those in other stars of close effective temperature. The high-excitation levels are depopulated in the line-formation layers due to photon loss in transitions to low-lying levels in $T_{\rm eff} \leq$ 10400 K model atmospheres and due to overionization of Si II in hotter atmospheres. For each transition, the lower level is depopulated to a greater extent than the upper level, resulting in a weakened line compared with its LTE strength (Fig. 6 for 6239 Å). NLTE effects grow toward higher $T_{\rm eff}$. For example, for Si II 6239 Å, $\Delta_{\rm NLTE} = 0.03$, 0.16 and 0.40 dex for HD 72660, 21 Peg and π Cet, respectively, and the line appears in emission in ι Her. In this hottest star of our sample, only 4621.7 and 5466.8 Å among the high-excitation lines are observed in absorption, although they are greatly weakened by NLTE effects, with $\Delta_{\rm NLTE} = 0.65$ and 1.18 dex, respectively. The lines on the long-wave side of 6239 Å either come into emission or disappear. They deserve special consideration in Section 6.3.

4.3.3 Lines of Si III

Observed lines of Si III (Table 5) arise from the transitions $4s\,^3S$–$4p\,^3P^\circ$ ($E_{\rm exc} = 19.02$ eV) and $4s\,^1S$–$4p\,^1P^\circ$ ($E_{\rm exc} = 19.72$ eV). In π Cet, only the first multiplet was measured; the lines are weak and form in deep atmospheric layers around $\log \tau_{5000} \sim -0.1$ (Fig. 1), where NLTE effects on the lines are caused by slight overpopulation of the lower level relative to its TE population. For Si III 4567 and 4574 Å, $\Delta_{\rm NLTE} = -0.13$ and −0.08 dex, respectively.

In ι Her, the Si III lines are stronger and form in the layers where the lower levels of both multiplets have enhanced excitation owing to pumping UV transitions from low-excitation levels, while the upper levels are depopulated via spontaneous transitions to the low-lying levels. Increasing the line absorption coefficient due to $b_{\rm low} > 1$ and dropping the line source function below the Planck function due to $b_{\rm up}/b_{\rm low} < 1$ results in strengthened lines and negative $\Delta_{\rm NLTE}$ of −0.18 to −0.35 dex for different lines.

4.4 Comparison with other NLTE studies

The NLTE abundances obtained can only be compared with the results of Wedemeyer (2001) for lines of Si II and Vega and Nieva & Przybilla (2012) for lines of Si III in ι Her. For the three Si II lines in common, namely 4128, 4130 and 5055 Å, the NLTE abundance corrections computed by Wedemeyer (2001) do not exceed 0.11 dex in absolute value and agree within 0.03 dex with ours. The NLTE abundances obtained in this study from individual lines of Si III in ι Her agree within 0.03–0.08 dex with those of Nieva & Przybilla (2012) and the mean abundances are consistent within 0.04 dex in the two studies.

5 ABUNDANCE ANALYSES OF $T_{\rm EFF} \leq$ 12 800 K STARS

For each of the eight stars with $T_{\rm eff} \leq$ 12800 K, its silicon spectrum is well reproduced in NLTE with a unique element abundance. The star ι Her, with both absorption and emission lines in its spectrum, is discussed in the next section. The average NLTE and

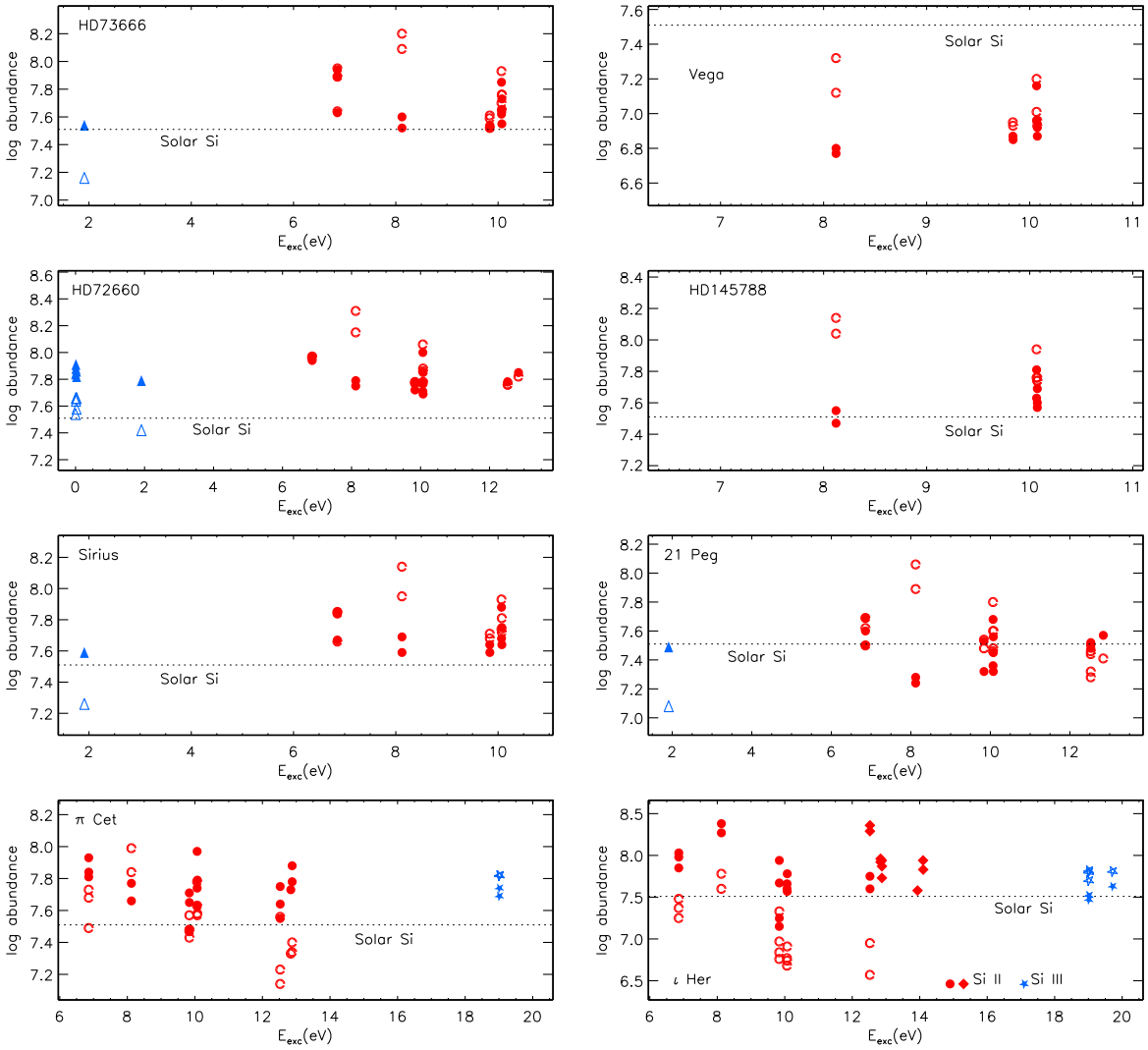

Figure 3. NLTE (filled symbols) and LTE (open symbols) abundances from individual lines of Si I (triangles), Si II (circles) and Si III (five-point stars) in the sample stars. For ι Her, the NLTE abundances derived from the Si II emission lines are shown by rhombi. The dotted line indicates the Solar system silicon abundance, $\log \varepsilon_{\odot} = 7.51 \pm 0.01$ (Lodders 2019).

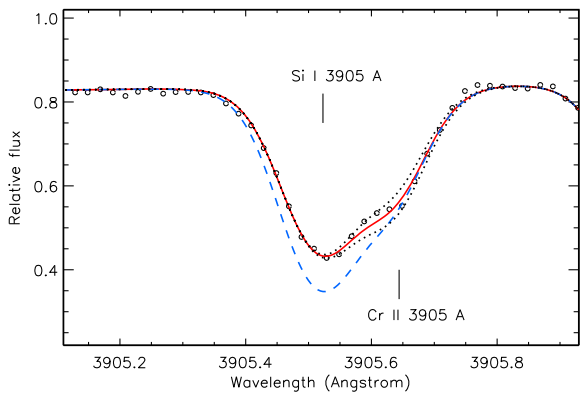

Figure 4. Best NLTE fit (solid curve) of Si I 3905 Å in HD 72660 (open circles). The corresponding LTE line profile is plotted by the dashed curve. The dotted curves show the NLTE synthetic spectra computed with 0.1 dex higher and lower abundance of Cr.

LTE abundances from each ionization stage observed in a given star are presented in Table 1.

We comment on the Si I lines in HD 32115. They reveal a substantial scatter of abundances, with $\sigma = 0.17$ dex, independent of either LTE or NLTE and independent of either measured equivalent widths (Fig. 2) or excitation potentials. Such a scatter is, most probably, due to the uncertainties in the *gf* values. Indeed, the dispersion was substantially reduced, down to $\sigma = 0.06$ dex, in a line-by-line differential approach, where from stellar line abundances we subtracted the individual abundances of their solar counterparts. The solar abundances (Table 2) were derived using the Kitt Peak Solar Flux Atlas (Kurucz et al. 1984) and calculations with the MARCS model atmosphere 5777/4.44/0 (Gustafsson et al. 2008) and a depth-independent microturbulence of 0.9 km s^{-1}.

For Si II in each star, NLTE reduces the line-to-line scatter substantially compared with the LTE case: for example, from $\sigma = 0.24$ to 0.08 dex for HD 32115 (four Si II lines) and from $\sigma = 0.25$ to 0.14 dex for π Cet (19 lines).

NLTE line formation is essential for achieving consistent abundances from Si I and Si II in the five stars where lines of both

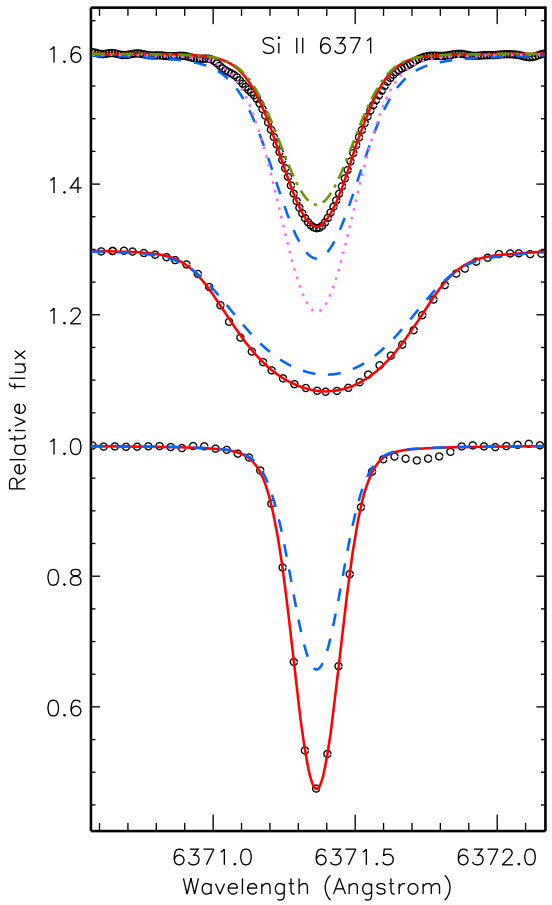

Figure 5. Best NLTE fits (solid curve) of Si II 6371 Å in ι Her, π Cet and 21 Peg (open circles, from top down). The corresponding LTE line profiles are plotted by the dashed curves. For ι Her, we also show the NLTE line profiles computed by replacing the electron-impact excitation data of Aggarwal & Keenan (2014) with the van Regemorter (1962) approximation for the allowed transitions and $\Upsilon = 1$ for the forbidden transitions (dash–dotted curve) and by replacing the TOPbase photoionization cross-sections for the Si II $4s\,^2S$, $3d\,^2D$ and $3p^2\,^2D$ levels with the hydrogenic ones (dotted curve). For better visibility, spectra of π Cet and ι Her are shifted along the Y axis.

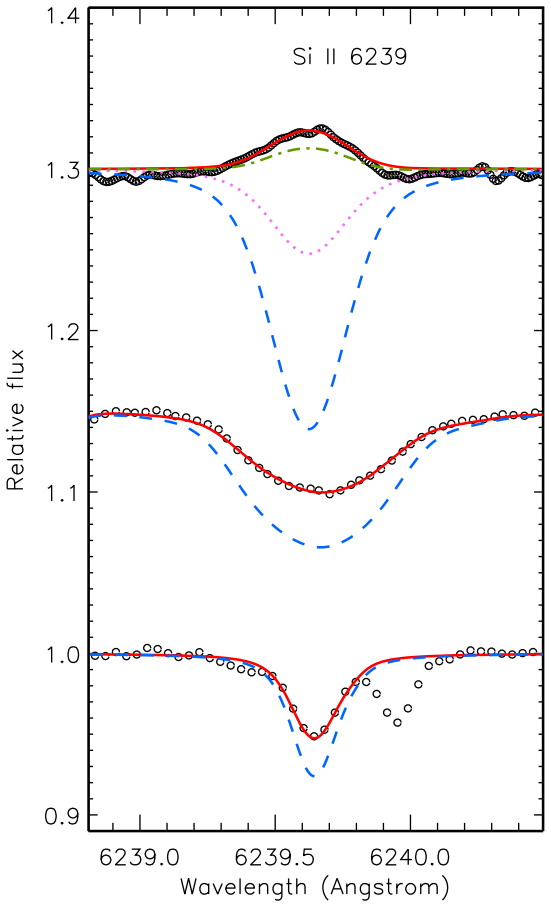

Figure 6. The same as in Fig. 5 for Si II 6239 Å.

ionization stages were measured. For example, the abundance difference (Si I – Si II) $= -0.07$ and -0.21 dex in NLTE and LTE, respectively, for HD 32115, and the corresponding numbers are -0.01 and -0.54 dex for 21 Peg. Fairly consistent NLTE abundances from lines of Si II and Si III were found in π Cet, while in LTE the abundance difference amounts to -0.23 dex.

The [Si/H] values were computed using the solar Si abundance, $\log \varepsilon_\odot = 7.51 \pm 0.01$, as recommended by Lodders (2019). For the stellar Si abundance, we computed the average value, if silicon was observed in the two ionization stages. The exception is Sirius. We relied on its Si II based abundance, having in mind that the only measured Si I line is affected by the Cr II line (see Fig. 4 for HD 72660) and Sirius is an Am star. We found that the silicon abundance follows the iron one in our sample stars, including λ Boo star Vega and the three Fe-rich stars, with the exception of π Cet. This suggests that the mechanisms that produced deviations in metal abundances of our chemically peculiar stars from the solar one did not separate chemical elements. For π Cet, with [Fe/H] $= 0$, according to Fossati et al. (2009), we found a supersolar

Table 6. Emission lines of Si II in ι Her.

Transition	$E_{\rm exc}$ [eV]	λ [Å]	$\log gf$	$\log \varepsilon$ NLTE
$4f\,^2F^\circ$–$6g\,^2G$	12.84	6239.61	0.18	7.92
		6239.61	−1.12	
		6239.66	0.02	
$5p\,^2P^\circ$–$6d\,^2D$	12.88	6818.41	−0.52	7.94
		6829.80	−0.26	7.87
		6829.83	−1.22	
$4d\,^2D$–$5f\,^2F^\circ$	12.52	7848.82	0.32	8.36
		7849.72	0.47	8.29
		7849.62	−0.83	
$5p\,^2P^\circ$–$7s\,^2S$	12.88	7125.85	−0.79	7.73
$5f\,^2F^\circ$–$9g\,^2G$	14.10	7911.52	−0.42	7.83
		7911.63	−0.60	
$5d\,^2D$–$8f\,^2F^\circ$	13.94	8044.41	−0.59	7.58
		8044.55	−0.44	
$5f\,^2F^\circ$–$8g\,^2G$	14.10	8935.50	−0.12	7.94
		8935.63	−0.30	
$4f\,^2F^\circ$–$5g\,^2G$	12.84	9412.66	1.23	7.96
		9412.66	−0.31	
		9412.78	1.12	

Notes. See text for sources of *gf* values.

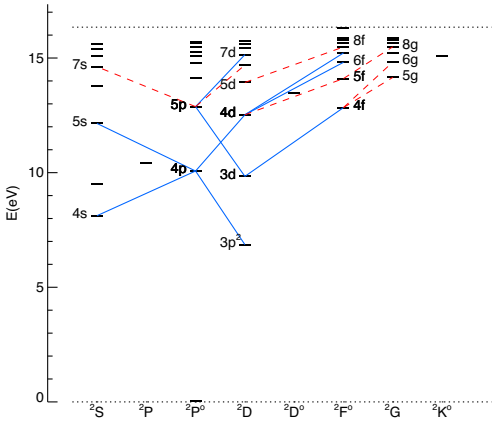

Figure 7. The doublet terms in the model atom of Si II. The absorption and emission spectral lines observed in ι Her arise from the transitions shown as continuous and dashed lines, respectively.

abundance of [Si/H] $=0.23$ from lines of both ionization stages, Si II and Si III.

6 NLTE ANALYSIS OF ι HER

6.1 Silicon absorption lines

NLTE reduces σ of the Si II based abundance; however, the line-to-line scatter remains uncomfortably large (Fig. 3). It is largely contributed by lines of the two multiplets 3853–3862 Å ($E_{\rm exc}$ = 6.86 eV) and 6347–6371 Å ($E_{\rm exc}$ = 8.12 eV). For example, for Si II in NLTE, we obtained σ = 0.50 dex when taking Si II 6347–6371 Å into account and σ = 0.25 dex without these two lines. In order to be consistent with the other lines, Si II 6347 and 6371 Å need to be strengthened in NLTE, as shown in Fig. 5 for a model where the TOPbase photoionization cross-sections were replaced with hydrogenic ones for the Si II 4s, 3d and 3p^2 ^{2}D levels. Such a change in NLTE effects compared with those for our standard model atom can be understood. From inspecting the NET $= n_l R_{lu} - n_u R_{ul}$ rates for b–f transitions of Si II, it was found that overionization of exactly these three levels is the main driver of overall overionization of Si II. Here, R_{lu} and R_{ul} are the radiative rates of the $l-u$ and reverse transitions, respectively. For the Si II 4s and 3d levels, their hydrogenic photoionization cross-sections are smaller than the TOPbase ones by more than one order of magnitude near the thresholds. Therefore, their use results in weakened NLTE effects for Si II and fits better to Si II 6347, 6371 Å. However, with such an atomic model we cannot reproduce the Si II emission lines (see Section 6.3).

Even without these two lines, the Si II based abundance is higher than that from the Si III lines, by 0.20 dex. For comparison, under the LTE assumption, an abundance difference between Si II and Si III amounts to −0.72 dex. When relying on the Si III lines, a close-to-solar silicon abundance of [Si/H] $= 0.03 \pm 0.07$ was obtained for ι Her, in line with the earlier determinations of Nieva & Przybilla (2012).

6.2 Uncertainties in derived abundances

We checked the sensitivity of NLTE abundances from representative lines of Si II and Si III to variations in atomic model and atmospheric parameters. Table 6 summarizes the results of our tests.

The NLTE effects for Si II 6347, 6371 Å were found to be rather stable. Variations in photoionization cross-sections and collisional rates produce abundance shifts of up to 0.07 dex. A substantial reduction of $\Delta_{\rm NLTE}$, by 0.33 dex, was obtained only in the case where oscillator strengths of the pumping 3p ^{2}P°–3p^2 ^{2}D (1808–1817 Å), 3p^2 ^{2}S (1304–1309 Å) and 4s ^{2}S (1526–1533 Å) transitions were increased by a factor of 10. Such a high uncertainty in f_{lu} is unlikely. We conclude that we are not able to treat the formation of Si II 6347, 6371 Å in ι Her correctly. These two lines were not accounted for when computing the mean abundance from the Si II lines.

Nieva & Przybilla (2012) estimate the uncertainties in $T_{\rm eff}$, log g and $\xi_{\rm t}$ as 200 K, 0.05 dex and 1 km s^{-1}, respectively. A downward revision of $T_{\rm eff}$ would reduce the mean abundance from lines of Si II by 0.03 dex and, in contrast, would increase the mean abundance for Si III by 0.08 dex, removing, in part, a discrepancy between Si II and Si III. Upward revision of log g would act in the same direction; however, the abundance shifts are smaller.

For the majority of the Si II lines in ι Her, we use $\Gamma_4/N_{\rm e}$ values from the laboratory measurements of Bukvić et al. (2009). They are proven to work well for stars (Section 5) where the quadratic Stark effect broadening is stronger than for ι Her. The approximate formula of Cowley (1971) was applied for lines of Si III. A reduction of Γ_4 by a factor of two would increase the Si III based abundance by 0.05 dex (Table 6).

Thus, the abundance difference obtained between Si II (without 6347, 6371 Å) and Si III can arise due to uncertainties in atmospheric parameters and line data.

6.3 Origin of Si II emission lines

Ten lines of Si II, which arise from transitions between the high-excitation doublet terms (Fig. 7), reveal emission or disappear in the spectrum of ι Her. They are listed in Table 7 and, in part, displayed in Figs 6 and 8. Their gf values are based on the calculations of Mendoza et al. (1995), as presented by NIST. An exception is the Si II 9412 Å triplet. NIST provides log $gf = -0.306$ for the only line, which arises from the transition between the $J_{\rm low} = 7/2$ and $J_{\rm up} = 7/2$ sublevels. In order to obtain the gf values given in Table 7, we used the calculations of R. Kurucz for all three lines of this triplet, as available in VALD: log gf = 1.012 (7/2–9/2), −0.532 (7/2–7/2) and 0.899 (5/2–7/2), and applied their gf ratios to the known NIST value.

The detected emission features are of photospheric origin and are naturally explained by interlocked NLTE effects acting in a photosphere, like the emission lines of C I (Alexeeva et al. 2016) and Ca II (Sitnova et al. 2018) in ι Her. The main driving mechanism of emission is overionization of Si II. As shown in Fig. 1 (bottom panel), the lower level of each emission transition is depopulated to a greater extent than the upper level in the line-formation layers, resulting in a line source function that rises relative to the local Planck function with photospheric height. It is essential that the NLTE correction to stimulated emission is sensitive to small deviations of the departure coefficients from unity whenever $h\nu \ll kT$. This explains why, in transitions from a common lower level, 4d, the shorter wavelength lines at 4621 and 5466 Å appear in absorption, although greatly weakened compared with their LTE strengths, while the near-IR lines at 7848, 7849 Å are in emission.

We checked how the emission mechanism is stable with respect to variations in atomic data. Table 6 shows the abundance shifts for Si II 6239 Å in part of all the tests made. Increasing photoionization cross-sections, within their uncertainties (10 per cent for the

Table 7. Error estimates for NLTE calculations of the silicon lines in ι Her.

		Changes in $\log \varepsilon_{Si}$ (dex)				
		Si II				Si III
		3856 Å	5978 Å	6239 Å	6371 Å	4567 Å
Atmospheric parameters:						
$T_{\rm eff}$ −200 K	$\sigma_{T_{\rm eff}}$	− 0.02	− 0.05	+ 0.07	− 0.06	+ 0.06
log g + 0.05	$\sigma_{\log g}$	− 0.02	− 0.01	+ 0.02	− 0.01	+ 0.04
$\xi_{\rm t}$ + 0.5 km s^{-1}	σ_{ξ}	− 0.08	− 0.01	0.00	− 0.06	− 0.04
Line data: $\Gamma_4 \times 0.5$	σ_{Γ}	+ 0.05	+ 0.01	0.00	+ 0.04	+ 0.05
Photoionizations:						
cross-sections × 1.1	$\sigma_{\rm RBF}$	0.00	− 0.01	+ 0.01	0.00	0.00
cross-sections × 2		− 0.02	− 0.03	+ 0.02	− 0.01	0.00
Si II $3p\,^2P^\circ$–$3p^2\,^2D$, $3p^2\,^2S$, $4s\,^2S$ transitions:						
$f_{lu} \times 10$		+ 0.16	− 0.04	+ 0.03	− 0.33	0.00
Collisional transitions:						
(Υ and $C_{\rm vR}$) × 2		− 0.01	+ 0.03	abs	0.00	0.00
(Υ and $C_{\rm vR}$) × 0.5	$\sigma_{\rm CBB}$	+ 0.01	− 0.05	− 0.50	0.00	0.00
(Υ, $C_{\rm vR}$ and $C_{\rm AK}$) × 2		− 0.02	− 0.03	abs	− 0.07	0.00
$\Delta_{\rm NLTE}$		0.55	0.83	e	0.67	− 0.28

Notes. $C_{\rm vR}$ = van Regemorter (1962) rates; $C_{\rm AK}$ = Aggarwal & Keenan (2014) rates; abs = absorption is predicted; e = emission line; 0.00 means smaller than 0.01 in absolute value.

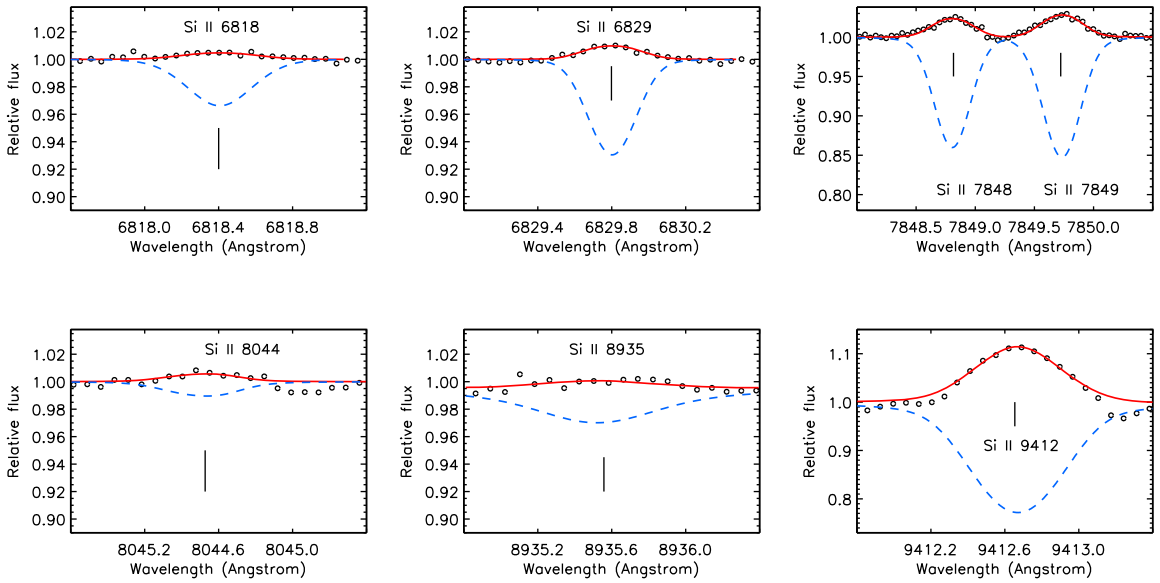

Figure 8. Best NLTE fits (solid curves) of the emission Si II lines in ι Her (open circles). The Si abundances obtained are presented in Table 4. The corresponding LTE line profiles are shown by dashed curves.

Table 8. NLTE abundance corrections (dex) for lines of Si I in the grid of model atmospheres.

λ [Å]	$T_{\rm eff}$ [kK], log g = 4.0		
	7	8	9
5948	−0.04	0.02	0.46
6155	−0.03	− 0.00	0.16
7405	−0.05	− 0.01	0.24

*Note.*This table is available in its entirety in a machine-readable form in the online journal. A portion is shown here for guidance regarding its form and content.

TOPbase data), and even doubling them has a minor effect on the emission phenomenon. The effect is strong, so that emission in the Si II lines disappears when the TOPbase photoionization cross-sections are either reduced by a factor of 10 or replaced, in part (for the Si II 4s, 3d and $3p^2\,^2D$ levels, Fig. 6), with hydrogenic ones.

Another set of test calculations was performed by varying collisional recipes: (i) the electron-impact excitation data of Aggarwal & Keenan (2014) were replaced with the van Regemorter (1962) semi-empirical approximation for allowed transitions and Υ = 1 for forbidden transitions (Fig. 6 for Si II 6239 Å); (ii) and (iii) the electron-impact ionization rates were scaled by factors of 0.1 and 10; (iv) for each b–b transition, its collisional rate was scaled by a factor of 2; (v), (vi) and (vii) for the transitions missing in Aggarwal & Keenan (2014), the van Regemorter (1962) rates and the standard Υ = 1 value were scaled by factors of 0.1, 0.5 and 2. Results of tests (iv), (vi) and (vii) for Si II 6239 Å are given in Table 6. Emission in Si II 6239 Å disappears, either to decrease the electron-impact

Table 9. NLTE abundance corrections (dex) for lines of Si I, Si II and Si III in the grid of model atmospheres.

λ [Å]	$T_{\rm eff}$ [kK], log g = 4.0													
	7	8	9	10	11	12	13	14	15	16	17	18	19	20
Si I														
3905	−0.01	0.03	0.34	0.43	0.36	0.39	0.42							
Si II														
5978	−0.02	−0.03	−0.07	−0.10	−0.10	−0.03	0.13	0.32	0.49	0.70	0.78	0.84	0.87	0.90
6239			0.05	0.07	0.14	0.27	0.54	1.07	1.12	1.17		e	e	e
6371	−0.16	−0.20	−0.35	−0.35	−0.31	−0.23	−0.09	0.07	0.21	0.46	0.63	0.78	0.90	1.01
Si III														
4567						−0.05	−0.08	−0.11	−0.13	−0.18	−0.21	−0.25	−0.29	−0.33

*Note.*For a given line, $\Delta_{\rm NLTE}$ is provided if the NLTE equivalent width exceeds 3 mÅ. e = emission line. This table is available in its entirety in a machine-readable form in the online journal. A portion is shown here for guidance regarding its form and content.

ionization rates (ii) or to increase the electron-impact excitation rates (iv, vii). The remaining tests keep emission in the Si II lines, although the best line profile fits are achieved with different element abundances for different collisional recipes.

Using our standard model atom, we derived the NLTE abundances from fitting the emission-line profiles (Table 7 and Fig. 3). They lie between $\log \varepsilon = 7.58$, which is close to the Si III based abundance, and the substantially higher value $\log \varepsilon = 8.36$. Our test calculations show that the magnitude of emission is very sensitive to variation in collisional rates for high-excitation transitions. Exactly those transitions are missing in the calculations of Aggarwal & Keenan (2014) that include the levels below $5p\,^2P^\circ$. Extended calculations of electron-impact excitation cross-sections for Si II are highly desirable to achieve consistent abundances from different emission lines.

Sadakane & Nishimura (2019) registered 12 emission lines of Si II in ι Her. Our NLTE calculations reproduce ten of them (Table 7). For the remaining two lines, at 5688 and 5701 Å, the NLTE calculations predict too strong emission. In order to fit the observations, one needs to reduce the Si abundance compared with the solar value by more than one order of magnitude. Both lines arise from the transition $3p3d\,^4F^\circ$–$3p4p\,^4D$, with $E_{\rm exc} > 14$ eV for the lower level. The majority of the quartet atomic terms have energies higher than the ionization energy of the Si II ground state, so that our model atom includes a few number (seven) quartet terms. These levels are weakly coupled to the doublet terms, mostly via collisional processes, and their populations are more dependent on the transitions between quartet levels. Since the system of quartet terms in our model atom is certainly incomplete, we cannot compute their populations correctly. For example, our NLTE calculations predict emission for the multiplet 6665, 6671, 6699 Å ($3p4s\,^4P^\circ$–$3p4p\,^4D$), while these lines are observed in absorption.

7 NLTE ABUNDANCE CORRECTIONS DEPENDING ON ATMOSPHERIC PARAMETERS

Our analyses of the silicon lines in the nine stars with well-determined atmospheric parameters provide evidence for the correct treatment of NLTE line formation for Si I–II–III through a range of A–B spectral types. Therefore, we can recommend users to apply the NLTE abundance corrections computed in this study in their research. These corrections are available for the lines listed in Tables 2 (Si I), 4 (Si I 3905 Å and Si II) and 5 (Si III). For calculations of $\Delta_{\rm NLTE}$, model atmospheres with solar metallicity and $\log g = 3.5$, 4.0 and 4.5 were taken from Kurucz's grid.[7] For Si I, Si II and Si III, $T_{\rm eff}$ varies between 7000 and 9000 K, 7000 and 20 000 K, and 12 000 and 20 000 K, respectively, with a step of 1000 K. Tables 8 and 9 and Fig. 9 present, in part, the computed $\Delta_{\rm NLTE}$ values.

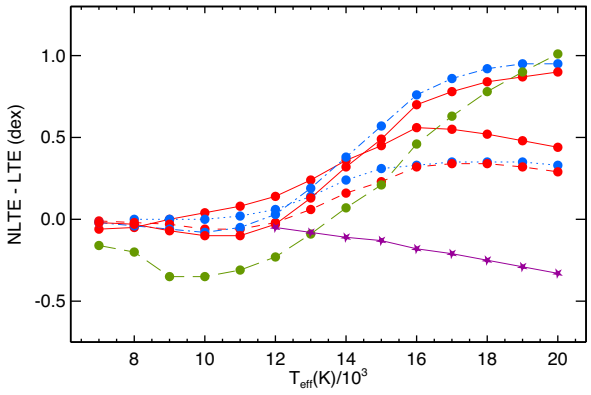

Figure 9. NLTE abundance corrections for Si II lines (circles) and Si III 4567 Å (five-point stars) depending on $T_{\rm eff}$ in the models with common $\log g = 4.0$ and solar metallicity. Different type curves correspond to different lines of Si II: 3862 Å (solid), 4075 Å (dotted), 4128 Å (short-dashed), 5055 Å (dot–dashed), 5978 Å (three-dot–dashed) and 6371 Å (long-dashed).

For the lines lying in the wings of the hydrogen lines, that is, Si I 3905 Å and Si II 3853, 3856, 3862, 4075, 4076, 4128 and 4130 Å, we recommend determining abundances using the NLTE spectral synthesis method, but not simply adding the NLTE corrections to the LTE abundances. Our $\Delta_{\rm NLTE}$ for Si II 6347, 6371 Å should be applied with caution in the case of stars as hot as ι Her (see Section 6.3).

8 CONCLUSIONS

This article presents a new comprehensive model atom of Si I–II–III that can be applied to NLTE analyses of Si I, Si II and Si III lines in a wide range of spectral types, where they are observed. Here, we performed NLTE calculations for a range of atmospheric parameters characteristic of unevolved A–B type stars: $T_{\rm eff} = 7000$–$20\,000$ K, $\log g = 3.5$, 4.0 and 4.5, and solar metallicity. The NLTE effects are different for lines of different ions in a given model atmosphere and they depend strongly on $T_{\rm eff}$.

For lines of Si I, NLTE effects are small for $T_{\rm eff} \leq 8000$ K, with slightly negative $\Delta_{\rm NLTE}$ at $T_{\rm eff} = 7000$ K and slightly positive $\Delta_{\rm NLTE}$

[7] http://kurucz.harvard.edu/grids/gridp00odfnew/

at $T_{\rm eff}$ = 8000 K. The $E_{\rm exc} > 4.9$ eV lines are weakened steeply with increasing $T_{\rm eff}$ and most of them cannot be measured in $T_{\rm eff} \sim 9000$ K stars. For the strongest of them and Si I 3905 Å, $\Delta_{\rm NLTE}$ grows towards higher $T_{\rm eff}$ and reaches 0.42 dex for Si I 3905 Å in the 13 000/4.0 model atmosphere.

The first ion of silicon is a majority species in the line-formation layers of the $T_{\rm eff} \leq 11\,000$ K models and is subject to overionization in hotter atmospheres. Except for Si II 6347, 6371 Å, NLTE effects are small for Si II lines, where Si II is a majority species. For different lines, $\Delta_{\rm NLTE}$ can be of different sign in a given atmosphere and does not exceed 0.1 dex in absolute value. The same lines in the $T_{\rm eff} \geq 12\,000$ K models are weakened compared with their LTE strengths due to overionization of Si II, resulting in positive $\Delta_{\rm NLTE}$, which grows with increasing $T_{\rm eff}$. For the Si II 3853–3862 Å, 4075–4076 Å and 4128–4130 Å multiplets, $\Delta_{\rm NLTE}$ reaches a maximal value at $T_{\rm eff}$ of about 17 000 K and decreases for higher $T_{\rm eff}$, due to shifting of the line formation depths to deeper atmospheric layers. NLTE effects are, in particular, large for the Si II 5041–5056 Å and 5957–5978 Å multiplets, with $\Delta_{\rm NLTE}$ of up 0.95 dex in the 20 000/4.0 model.

The Si II 6347, 6371 Å lines are greatly strengthened in NLTE over wide range of $T_{\rm eff}$, even in atmospheres where Si II is subject to overionization. For example, for Si II 6347 Å in the log g = 4.0 models, $\Delta_{\rm NLTE}$ reaches a most negative value of −0.40 dex for $T_{\rm eff}$ = 9000 and 10 000 K and turns positive for $T_{\rm eff} \geq 14\,000$ K.

Our NLTE calculations predict that, in $T_{\rm eff} \geq 17\,000$ K models, some lines of Si II, which arise from high-excitation (above $4d\,^2D$) doublet levels, come into emission due to the NLTE effects acting in an atmosphere. The main driving mechanism of emission is overionization of Si II.

NLTE abundance corrections for Si III lines are negative in the stellar parameter range with which we are concerned and increase, in absolute value, towards higher $T_{\rm eff}$.

The new model atom was tested with nine unevolved A9–B3 type stars, with well-determined atmospheric parameters and high-resolution observed spectra available. The hottest star, ι Her, is known for many emission lines of various chemical species, including 12 lines of Si II (Sadakane & Nishimura 2019). Our NLTE calculations with a classical hydrostatic model that represents the atmosphere of ι Her reproduced ten of them, although using rather different element abundances for different lines. The magnitude of emission is sensitive to variation in collisional rates. Accurate electron-impact excitation cross-sections for the Si II transitions between the high-excitation levels are highly desirable, in order to achieve consistent abundances from different emission lines.

For each star, the NLTE and LTE abundances were determined from the absorption lines. NLTE reduces the line-to-line scatter for Si II substantially compared with the LTE case and leads to consistent mean abundances from lines of different ionization stages. For example, in NLTE and LTE, the Si I–Si II abundance difference in 21 Peg amounts to −0.01 and −0.54 dex, respectively, and the Si II–Si III difference in ι Her is + 0.20 and −0.72 dex. Thus, with the new model atom, the line formation for Si I–Si II–Si III in atmospheres of A- to mid B-type stars is treated correctly. The exception is the Si II 6347, 6371 Å doublet in ι Her, for which NLTE effects are overestimated. They NLTE effects are stable with respect to variations in photoionization cross-sections and electron-impact excitation data. At this stage, we failed to understand this problem and further theoretical work is required.

We obtained the result that, except for π Cet, the silicon abundance follows the iron one in our sample stars, including λ Boo star Vega and Am stars HD 72660 and Sirius. This suggests that the mechanisms that produced deviations from the solar values in the metal abundances of our chemically peculiar stars did not separate chemical elements. A supersolar abundance of [Si/H] = 0.23 was found from lines of the two ionization stages, Si II and Si III, for π Cet, which has [Fe/H] = 0, according to Fossati et al. (2009). A NLTE study of the iron lines in A- to mid B-type stars is in progress (Sitnova et al., in preparation).

ACKNOWLEDGEMENTS

The author thanks K.M. Aggarwal for providing effective collision strengths for the Si II transitions, T. Ryabchikova for providing the observed spectra and model atmospheres computed with the code LLMODELS and J. Landstreet for providing the UV spectrum of HD 72660. This study made use of the ESO UVESPOP, NIST, TOPbase, NORAD, open-ADAS,[8] VALD, ADS[9] and R. Kurucz's databases.

REFERENCES

Aggarwal K. M., Keenan F. P., 2014, MNRAS, 442, 388
Alexeeva S. A., Ryabchikova T. A., Mashonkina L. I., 2016, MNRAS, 462, 1123
Alexeeva S., Ryabchikova T., Mashonkina L., Hu S., 2018, ApJ, 866, 153
Amarsi A. M., Asplund M., 2017, MNRAS, 464, 264
Bailey J. D., Landstreet J. D., 2013, A&A, 551, A30
Bard S., Carlsson M., 2008, ApJ, 682, 1376
Becker S. R., Butler K., 1990, A&A, 235, 326
Bergemann M., Kudritzki R.-P., Würl M., Plez B., Davies B., Gazak Z., 2013, ApJ, 764, 115
Blanco F., Botho B., Campos J., 1995, Phys. Scr., 52, 628
Bukvić S., Djeniže S., Srećković A., 2009, A&A, 508, 491
Butler K., Giddings J., 1985, Newsletter on the Analysis of Astronomical Spectra, No. 9. University of London, London, UK
Castelli F., Kurucz R. L., 1993, in Dworetsky M. M., Castelli F., Faraggiana R., eds, ASP Conf. Ser. Vol. 44, IAU Colloq. 138, Peculiar versus Normal Phenomena in A-type and Related Stars. Astronomical Society of the Pacific, San-Francisco, CA, p. 496
Cowley C. R., 1971, The Observatory, 91, 139
Cunto W., Mendoza C., Ochsenbein F., Zeippen C. J., 1993, A&A, 275, L5
Fernández-Menchero L., Del Zanna G., Badnell N. R., 2014, A&A, 572, A115
Finn G. D., McAllister H. C., 1978, Sol. Phys., 56, 263
Fossati L., Bagnulo S., Monier R., Khan S. A., Kochukhov O., Landstreet J., Wade G., Weiss W., 2007, A&A, 476, 911
Fossati L., Ryabchikova T., Bagnulo S., Alecian E., Grunhut J., Kochukhov O., Wade G., 2009, A&A, 503, 945
Fossati L., Ryabchikova T., Shulyak D. V., Haswell C. A., Elmasli A., Pandey C. P., Barnes T. G., Zwintz K., 2011, MNRAS, 417, 495
Garz T., 1973, A&A, 26, 471
Golriz S. S., Landstreet J. D., 2016, MNRAS, 456, 3318
Gustafsson B., Edvardsson B., Eriksson K., Jorgensen U. G., Nordlund Å., Plez B., 2008, A&A, 486, 951
Hill G. M., Landstreet J. D., 1993, A&A, 276, 142
Hubeny I., Hummer D. G., Lanz T., 1994, A&A, 282, 151
Hummer D. G., Mihalas D., 1988, ApJ, 331, 794
Kamp L. W., 1978, ApJS, 36, 143
Kramida A., Ralchenko Y., Reader J., NIST ASD Team, 2019, NIST Atomic Spectra Database (version 5.7.1). Gaithersburg MD, USA http://physics.nist.gov/asd, National Institute of Standards and Technology
Kurucz R. L., Furenlid I., Brault J., Testerman L., 1984, Solar Flux Atlas from 296 to 1300 nm. National Solar Observatory, New Mexico

[8] http://open.adas. ac.uk
[9] http://adsabs.harvard.edu/abstract_service.html

Lennon D. J., Brown P. J. F., Dufton P. L., Lynas-Gray A. E., 1986, MNRAS, 222, 719
Lodders K., 2019, preprint (arXiv:1912.00844)
Martin W. C., Zalubas R., 1983, Journal of Physical and Chemical Reference Data, 12, 323
Matheron P., Escarguel A., Redon R., Lesage A., Richou J., 2001, J. Quant. Spec. Radiat. Transf., 69, 535
Mendoza C., Eissner W., LeDourneuf M., Zeippen C. J., 1995, Journal of Physics B: Atomic Molecular Physics, 28, 3485
Mihalas D., Hummer D. G., Conti P. S., 1972, ApJ, 175, L99
Nahar S. N., 1995, ApJS, 101, 423
Nahar S. N., 2000, ApJS, 126, 537
Nayfonov A., Däppen W., Hummer D. G., Mihalas D., 1999, ApJ, 526, 451
Nieva M.-F., Przybilla N., 2012, A&A, 539, A143
O'brian T. R., Lawler J. E., 1991, Phys. Rev. A, 44, 7134
Przybilla N., Nieva M.-F., Butler K., 2008, ApJ, 688, L103
Przybilla N., Nieva M.-F., Butler K., 2011, Journal of Physics Conference Series, 328, 012015
Ryabchikova T., Piskunov N., Kurucz R. L., Stempels H. C., Heiter U., Pakhomov Y., Barklem P. S., 2015, Phys. Scr., 90, 054005
Sadakane K., Nishimura M., 2017, PASJ, 69, 48
Sadakane K., Nishimura M., 2019, PASJ, 71, 45
Seaton M. J., 1962, in Bates D. R., ed., Atomic and Molecular Processes. Academic Press, New York and London, p. 375
Seaton M. J., 1987, Journal of Physics B: Atomic Molecular Physics, 20, 6363
Shchukina N., Sukhorukov A., Trujillo Bueno J., 2012, ApJ, 755, 176
Shi J. R., Gehren T., Butler K., Mashonkina L. I., Zhao G., 2008, A&A, 486, 303
Shulyak D., Tsymbal V., Ryabchikova T., Stütz C., Weiss W. W., 2004, A&A, 428, 993
Singh J., Aggarwal S., Jha A. K. S., Singh A. K., Mohan M., 2011, Canadian Journal of Physics, 89, 1119
Sitnova T. M., Mashonkina L. I., Ryabchikova T. A., 2013, Astronomy Letters, 39, 126
Sitnova T. M., Mashonkina L. I., Ryabchikova T. A., 2016, MNRAS, 461, 1000
Sitnova T. M., Mashonkina L. I., Ryabchikova T. A., 2018, MNRAS, 477, 3343
Smith P. L., Huber M. C. E., Tozzi G. P., Griesinger H. E., Cardon B. L., Lombardi G. G., 1987, ApJ, 322, 573
Tsymbal V., , Ryabchikova T., Sitnova T., 2019, in Kudryavtsev D. O., Romanyuk I. I., Yakunin I. A., eds, ASP Conf. Ser. Vol. 518. Physics of Magnetic stars, San Francisco: Astronomical Society of the Pacific, p. 247
van Regemorter H., 1962, ApJ, 136, 906
Vernazza J. E., Avrett E. H., Loeser R., 1976, ApJS, 30, 1
Wedemeyer S., 2001, A&A, 373, 998
Wiese W. L., , Smith M. W., Miles B. M., 1969, Atomic Transition Probabilities. Vol. 2: Sodium through Calcium. A critical data compilation, National Bureau of Standards, Washington, D.C. 20402, USA .
Wilke R., 2003, Ph.D. Thesis. Heinrich-Heine-Universitat. Dusseldorf

SUPPORTING INFORMATION

Supplementary data are available at *MNRAS* online.

Table 8. NLTE abundance corrections (dex) for lines of Si I in the grid of model atmospheres.
Table 9. NLTE abundance corrections (dex) for lines of Si I, Si II and Si III in the grid of model atmospheres.

Please note: Oxford University Press is not responsible for the content or functionality of any supporting materials supplied by the authors. Any queries (other than missing material) should be directed to the corresponding author for the article.

This paper has been typeset from a TEX/LATEX file prepared by the author.